

# Enhancement on the Tool Steel's Surface Properties by Eta Carbide Distribution Mechanism of Cryogenic Treatment

Esad Kaya<sup>1</sup>  · Koray Kılıçay<sup>1</sup>  · Mustafa Ulutan<sup>1</sup> 

Received: 26 March 2020 / Accepted: 10 August 2020 / Published online: 28 August 2020  
© The Indian Institute of Metals - IIM 2020

**Abstract** In this study, the effect of cryogenic treatment on microstructural, mechanical, and tribological properties of AISI L2 steel was investigated. Heat treatment processes conducted were, as directly quenched (C), quenched tempered (CT), and quenched cryogenically treated (CC), and the last group (CCT) was additively tempered. The volume fraction of retained austenite, the percentage of carbide density, hardness, empiric fracture toughness, the coefficient of friction (COF), and adhesive/abrasive wear resistance were determined according to the relevant standards. The retained austenite ratio decreased for the CCT process which also reduced the distance between carbides, and it increased the carbide density. A drastic improvement was observed in the tribological behavior of CC and CCT samples. CCT process increased the operational service life of steel in mold making applications due to high adhesive wear resistance, while the CC process provided the best solution for cold cutting operations due to the highest abrasive wear resistance.

**Keywords** Friction · Heat treatment · Wear · Tool steel

## 1 Introduction

Cold-work tool steels have a wider usage area than any other tool steels group. Therefore, properties including wear resistance, hardness, toughness, hardenability, and homogeneous microstructure are expected to be superior.

These superior properties, and dimensional stability, can be provided by using different heat treatments [1]. Cryogenic treatment is one such method, which is still being developed. The cryogenic treatment can enhance specific properties of the materials such as hardness [2], wear resistance [3], tensile/bending strength [4], fatigue life [5], toughness [4], and operational tool life [6].

Researchers have performed cryogenic treatments on different materials, which include stainless steels [7], cast iron [8], cemented carbides [9], and nonferrous alloys [10]. Ramesh et al. [11] have studied the effect of cryogenic treatment and tempering on the corrosion and microstructure behavior of structural steel. They showed that cryogenic treatment enhances the martensite matrix rigidity. Liu et al. [12] have made a comparative study of the cryogenic treatment of valve steel. They observed that use of the cryogenic treatment, as a cycle, significantly reduces the retained austenite ratio. Senthilkumar [13] has researched the influence of cryogenic treatment on the mechanical behavior of high carbon EN31 steel. He found that the elimination of retained austenite, by the cryogenic treatment, increases the general matrix hardness. He also mentioned that with low-temperature tempering conditioning and cryogenic treatment together, samples show better toughness than as-quenched samples. Shinde and Dhokey [14] have researched the correlation between cryogenic treatment soaking time and carbide density, surface roughness, and dry sliding wear behavior, on AISI H13 hot work tool steel. They found that soaking time is a critical limit, which directly affects secondary carbide density. As can be seen from the literature review, cryogenic treatment provides outstanding improvements in the service life of machine parts and tools, which are exposed to high wear, impact, and corrosion.

✉ Esad Kaya  
esatkaya@ogu.edu.tr

<sup>1</sup> Department of Mechanical Engineering, Eskisehir Osmangazi University, Eskisehir, Turkey

A previous literature survey has shown that cryogenic treatment has a tremendous effect on ferrous alloy. However, recent studies carried out on cold-work tool steels are limited to the surface treatments, due to it being a specially designed high-carbon low-alloy steel. AISI L2 is generally used for cold cutting, drilling, and shaping operations. In these fields of use, damage and failures can cause many difficulties including casualties, increased manufacturing time, and high costs. For this reason, the current study examines the alteration in the microstructural and tribological properties of the AISI L2 steel after adding cryogenic treatment and tempering to the main conventional heat treatment procedures.

## 2 Materials and Methods

The chemical composition of the AISI L2 cold-work tool steel and the experimental procedure is shown in Table 1. Test samples were prepared with dimensions of  $20 \times 10 \times 100 \text{ mm}^3$ . All samples were austenitized at  $810 \text{ }^\circ\text{C}$  for 40 min and then quenched in an oil medium. Cryogenic treatments were performed at  $-196 \text{ }^\circ\text{C}$  for 36 h and were applied directly after the quenching. The temperature distribution of the cryogenic cooling chamber was monitored by a computer-controlled system (MMD Cryo). Tempering processes for all samples were performed for 1 h at  $200 \text{ }^\circ\text{C}$ . For metallographic examinations, all samples were ground, polished, and subsequently etched with a 2% Nital solution. The samples were examined using a scanning electron microscope (SEM, JEOL JSM-5600LV) and an elemental dispersive spectroscopy (EDS) technique. The phases in the microstructures were also analyzed by X-ray diffraction (XRD). Patterns were obtained by using a Bruker D8 Advance X-ray device in  $\text{Cu-K}_\alpha$  radiation mode. The scanning angle was selected as  $20^\circ$  to  $100^\circ$ . XRD patterns were analyzed by the X Powder diffraction indexing software, and the volume fraction of retained austenite

( $f_{\text{aust}}$ ) was calculated under ASTM-E975-03. The hardness of samples was measured under ASTM E18 by using a Zwick 3106 tester in the Rockwell C scale. Five hardness measurement values were taken for each sample, and the mean hardness value and deviation were determined. The percentage of carbide analysis was performed using an optical microscope (Nikon Clemex) with images taken on the  $500 \times$  magnification scale. Four microstructure images were used for the calculation. Mean carbide phase density ( $f_{\text{carb}}$ ) and mean diameter of carbides ( $D_p$ ) were determined using ImageJ analysis software. The distance between carbide particles ( $d_p$ ) was calculated using the following Eq. (1) [15]:

$$d_p = D_p(1 - f_{\text{carb}}) \sqrt{\frac{2}{3f_{\text{carb}}}} \quad (1)$$

The empiric fracture toughness ( $K_{1c}$ ) values were calculated using Eq. (2) [16]:

$$K_{1c} = 1.363 \left( \frac{\text{HRc}}{\text{HRc} - 53} \right) \left( \sqrt{E} \cdot d_p \frac{1}{\sqrt[6]{f_{\text{carb}}}} (1 + f_{\text{aust}}) \right) \quad (2)$$

Adhesive wear resistance and friction tests were performed with a pin-on-disk type method according to the ASTM G99 norm by using a CSM Tribometer. A 3 mm diameter of certified sphericity WC ball was used as the counter body. The disk was rotated in dry sliding conditions with a linear speed of 3 cm/s. Total wear test distance was 100 meters, with the coefficient of friction being recorded concurrently. After the adhesive wear test, the profile of the worn surface was measured by using a Mitutoyo SJ-400 profilometer. The wear rate was calculated from the four measured worn areas. The worn surface was examined with SEM, EDS, and surface roughness measurement analysis. The wear mechanism for all samples was determined with regard to the adhesive wear test. Abrasive wear tests were applied to the samples

**Table 1** The chemical composition of the AISI L2 steel and experimental procedure

C	Si	Mn	P	S	Cr	V
<i>Chemical composition (%wt.)</i>						
1.15	0.22	0.30	0.015	0.015	0.65	0.010
Samples	Quenching		Cryogenic treatment			Tempering
<i>Experimental procedure</i>						
C	+		-			-
CT	+		-			+
CC	+		+			-
CCT	+		+			+

in compliance with ASTM G77 by the Plint TE-53 tester. SiC abrasive paper (400 mesh density) was used as the counter body. Abrasive wear tests were performed under 42 N wear load, 400 meters wear distance, and 200 rpm rotation speed. Total weight losses were calculated by measuring the weight of the samples before and after the abrasive wear test. Abrasively worn surfaces were examined by SEM, EDS, and surface roughness measurement analysis, and tribological behaviors of the samples were investigated.

### 3 Result and Discussion

#### 3.1 Microstructure and Hardness

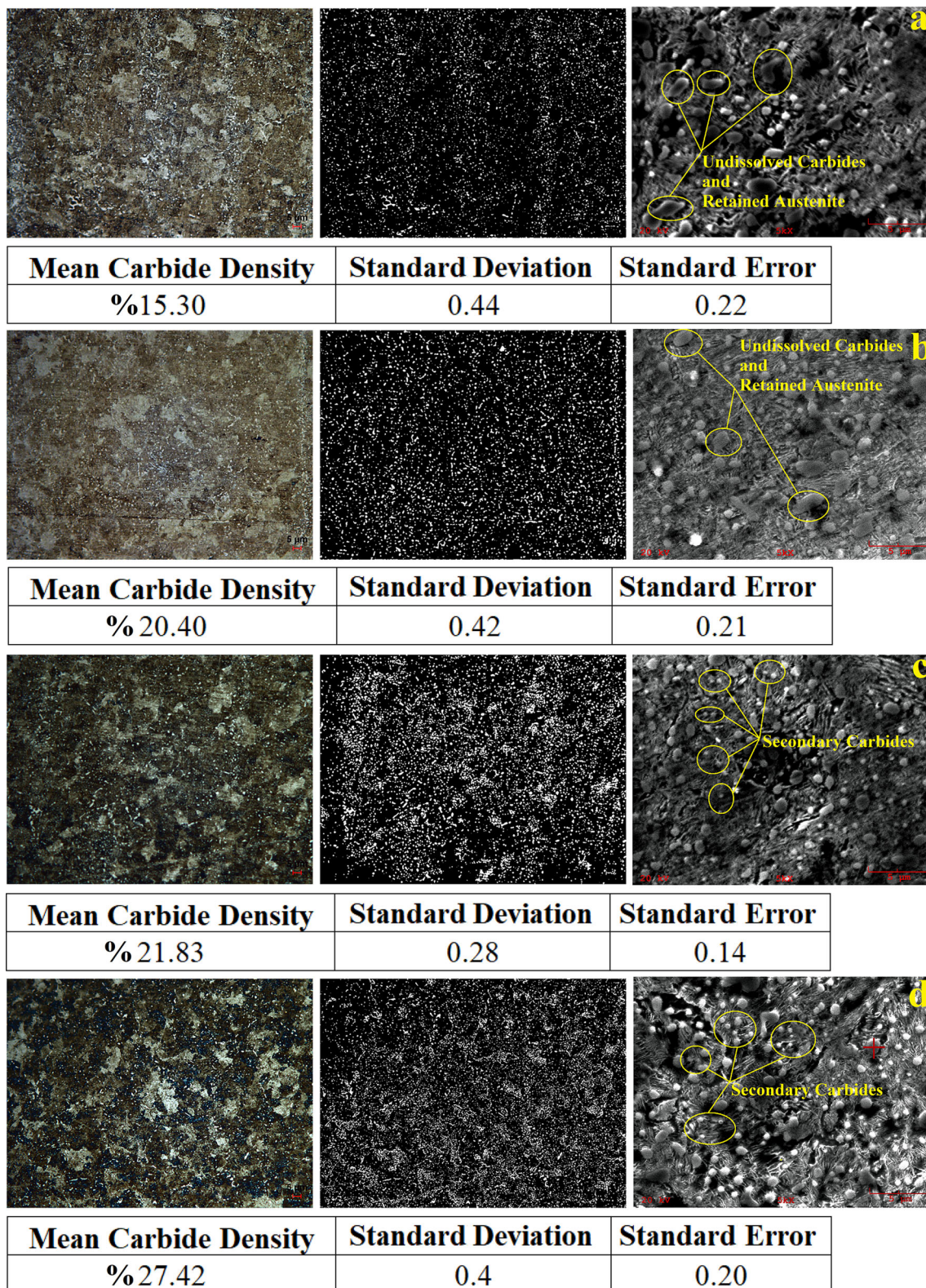
Figure 1 shows SEM photographs of all heat-treated samples. As can be seen from the micrographs, the general microstructure of all the samples consists of lath martensite, tempered martensite, carbides, and retained austenite phases. Referring to the as-quenched sample (Fig. 1a), the sample's microstructure get transformed into martensite by oil quenching. Retained austenite phase, undissolved coarse, and primary carbides can be seen in the microstructure. This indicates that the martensitic transformation is not completely achieved. Deficient martensitic transformation is the main problem for the heat treatment of tool steels. After quenching, it can be seen that the size of the carbides in the microstructure is considerably larger than that of cryogenically treated samples. Also, the carbides in the microstructure appear to be locally intense and have a nonhomogeneous distribution. The distribution, size, quantity, and distance between the particles of these carbides affect the mechanical properties of the material drastically. Therefore, the high grain size in tool steels does not provide the desired mechanical properties.

Figure 1b shows the microstructure of the CT sample. The reduction in the carbide size is achieved by tempering after quenching. As a result, the number of grain boundaries in the material is increased, and the carbide's shape take a round form. After tempering, carbon atoms are driven impelled from the martensite lattice, and a tempered martensite structure is formed. It is predicted that after tempering, the steel microstructure is tougher. In this case, the transformation of the martensite structure to tempered martensite also helps to remove the residual stresses. However, it can be seen that the primary carbide sizes are still too coarse compared with the CC and CCT samples (Fig. 1). Figure 1c shows the SEM microstructure of the CC group. It has been found that cryogenic treatment eliminates the amount of undissolved coarse and primary carbides and retain austenite in the microstructure. It can be

seen that the formed secondary carbides have better distribution in the microstructure in comparison with the C sample. The formed secondary carbides are thought to be small fragments of Fe content, which are mostly coarse and metastable. Depending on these formed secondary carbides, the microstructure is partially stabilized in comparison with the C and CT samples.

Figure 1d shows the microstructure of the CCT sample. When the microstructure is examined in detail, it can be seen that the primary phases in the microstructure are composed of lath type martensite. Also, various Cr and V content carbides are observed which are homogeneously distributed in the microstructure. The chemical content is measured as 0.98 wt% Cr and 0.22 wt% V (Fig. 1d EDS dot). It has also been found that the formed secondary carbides are mainly deposited on the grain boundaries compared to the other groups. The tempering process, which is done after cryogenic treatment, increases martensitic transformation and secondary carbide precipitation. This case has been confirmed by many researchers who have found that carbides bond much more tightly on the main matrix (lath martensite) during wear and impact [17, 18]. The precipitation of carbides depends on the correct selection of the tempering process temperature. Since the chosen tempering temperature is below 400 °C for AISI L2, the carbon atoms present in both face-centered cubic retained austenite and body-centered tetragonal martensite structure come out of the lattices due to the low-tempering temperature diffusion effect. In this case, they form secondary carbides with free alloying elements that are present in dislocations and spaces. These secondary, stabilized carbides (also known as  $\eta$ ), are precipitated due to the effect of the tempering process at a low temperature and help to increase the toughness by supporting the brittle and hard lath type of martensite matrix phase.

Figure 1 also shows that the carbide content threshold images are obtained by the mapping method, for the microstructures. In these photographs, the black regions show the martensite matrix, while the white regions show the coarse, primary, and secondary carbides in the microstructure. Figure 1 shows the obtained results of the carbide density, using the mapping method, from the microstructures of the samples. The highest carbide density is 27.42% in the CCT sample, while the lowest carbide density is calculated as 15.30% in the C sample. It is seen that the carbide densities of the CT and CC samples seem to be equivalent. This situation illustrates the importance of tempering after cryogenic treatment. It has also been found that the CCT process allows the carbides to be refined in the microstructure (Fig. 1d). It is implied that cryogenic treatment has a positive effect on microstructural properties.

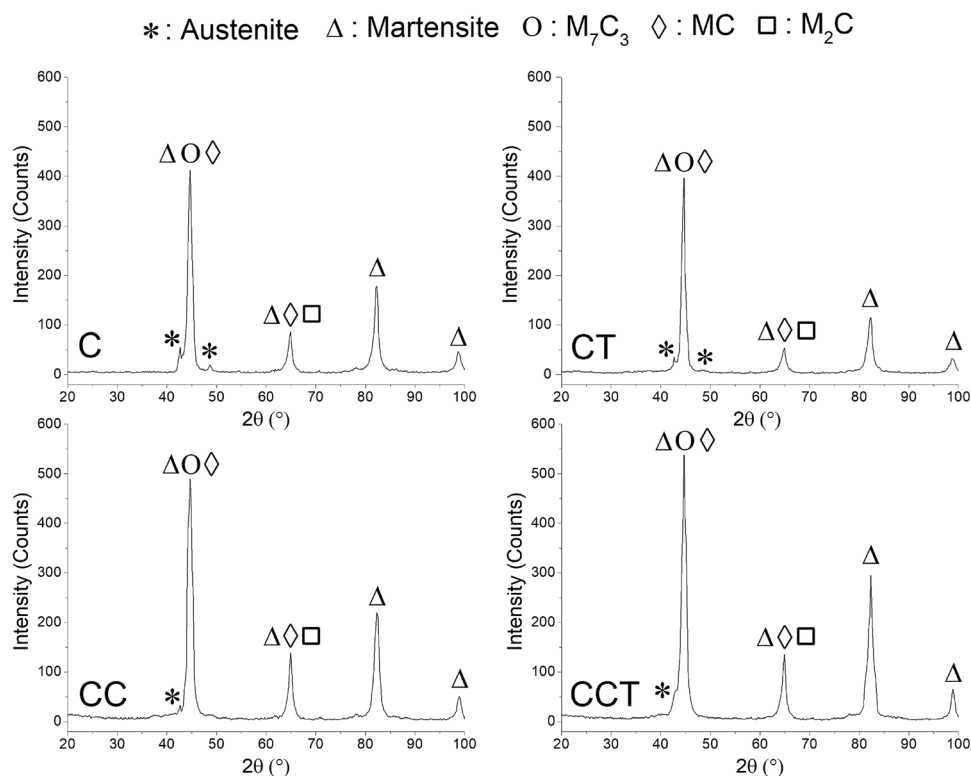


**Fig. 1** The mapping microstructures and EDS images of the samples, **a** C, **b** CT, **c** CC, **d** CCT

XRD analyses of the samples are shown in Fig. 2. The sample patterns contain austenite, martensite, MC,  $M_7C_3$ ,

and  $M_2C$  carbide phase's peaks. As can be seen from Fig. 2, the intensity of the austenite peaks decreases in the

**Fig. 2** X-ray diffraction patterns of the samples



cryogenically treated samples (CC and CCT). As the steel is high-carbon low-alloy steel, a slight reduction is observed in the intensity of austenite peaks. The percentage volume fraction of measured retained austenite ratios is determined from the XRD pattern by respectively, as 6.1%, 3.3%, 2.7%, and 0.9%. The lowest retained austenite ratio is observed in the CCT sample as 0.9%, while the highest retained austenite ratio is found in the C sample as 6.1%. By applying the cryogenic treatment and tempering process, the retained austenite ratio reduces sevenfold in the microstructure. This condition also validates the phenomena that there is a reduction in the retained austenite ratio by the application of cryogenic treatment. Martensite peak pattern analysis shows that the highest peak intensity of martensite is seen in the CCT sample. The peak at 44° contains carbides and martensite phases and is the highest intensity peak of all the samples. It can be seen that the intensity of this peak increases in the cryogenically treated samples (CC and CCT). A similar situation is seen for the peaks at 82° and 99°. It is also observed that the peak intensity of 64° increases in the cryogenically treated samples, which contain  $M_7C_3$ ,  $M_2C$  carbides, and martensite phases. As seen from XRD patterns, the density and the width of the carbide and martensite peaks of the cryogenically treated samples seem to be higher. This proves martensitic transformation and carbide precipitation.

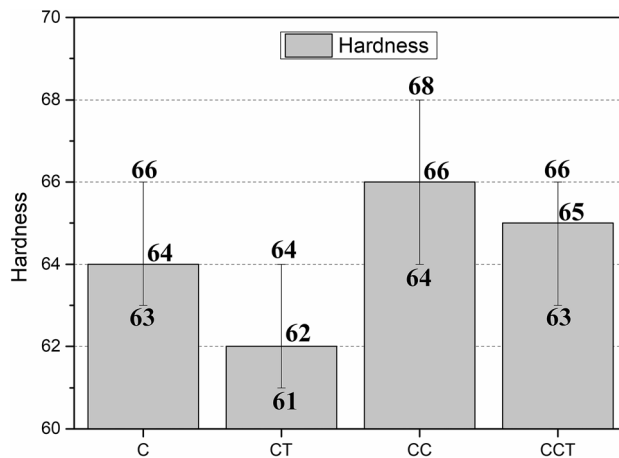


**Fig. 3** Hardness values (HRC) of the samples

Figure 3 shows the hardness values of all the samples. The hardness of the untreated sample is measured as 28 HRC. Due to quenching in the oil medium, the hardness of all heat-treated samples is higher than the untreated sample. For this reason, it is thought that quenching processes should be successfully performed. The average hardness values for all groups range from 62 to 66 HRC. The hardness values of the CCT sample are found to be nearly equivalent to the C sample. Compared with the CT sample, which has a tempered martensite phase, cryogenic treatment together with a tempering (CCT) is thought to

compensate for the loss of hardness due to tempering, with the help of the precipitation of secondary carbides and a full martensitic transformation. The highest hardness values are obtained in the CC sample. The martensitic transformation and secondary fine carbides precipitation are the major reason for this increase in hardness.

### 3.2 Fracture Toughness

Figure 4 shows the empirical fracture toughness ( $K_{1c}$ ) and the distance between carbides ( $d_p$ ) for all samples. Cryogenic treatment and tempering reduce the distance between carbides. Due to this situation, it is observed that the fracture toughness of the cryogenically treated samples decreases. Equations (1) and (2) have been used for the calculation of the distance between carbides and fracture toughness, respectively. Equation (1) shows that the  $d_p$  value is inversely proportional to carbide density. In agreement with microstructural mapping image analysis (Fig. 1), it is seen that the distance between carbides decreases for all the cryogenically treated samples. In terms of phase ratio, it is seen that the fracture toughness value is in proportion to the retained austenite ( $f_{aust}$ ) value in Eq. (2). This situation agrees with the decrease in fracture toughness relevant to the reduction in the distance between carbides for cryogenically treated samples. Other studies have shown that cryogenic treatment is known to increase the kinetics of carbide formation in steel materials [18–20]. It is seen that the obtained results, by empirical calculations, are in agreement with the theories on the effect of cryogenic treatment on steels.

### 3.3 Wear and Friction

The adhesive wear rates and the average coefficient of friction (COF) of different heat-treated samples are shown in Fig. 5a. The COF wear distance diagrams of the samples

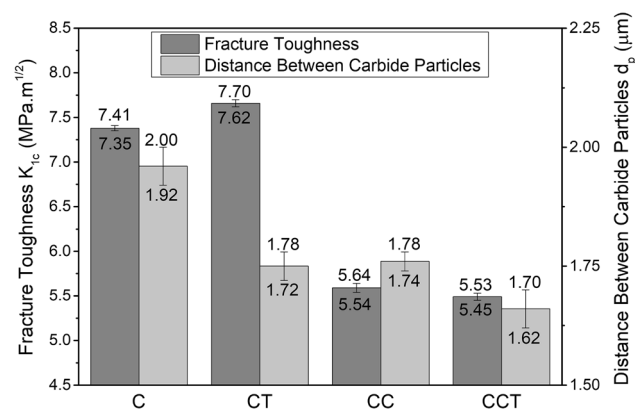


**Fig. 4** Empirical properties; Fracture toughness ( $K_{1c}$ ), and Distance between Carbides ( $d_p$ )

are shown in Fig. 6. The adhesive wear rates are reduced by about 1.2–3.6 times compared with the C sample. It is seen that the lowest mean COF value as observed in the CCT sample is 0.44. Other samples show similar fluctuating behavior of COF along with the distance as nearly in the range of 0.62 values. In Fig. 6, the COF values of C, CT, and CC samples increases after about 50 m possibly due to the poorly bonded carbides and broken oxide layers turning into moving abrasive particles in the tribological system. It can be estimated that oxide layers containing Fe and W are formed, with tribo-chemical reactions, on the worn surfaces of the C, CT, and CC samples. As a result, these oxide layers are separated from the surface with increasing wear distance and so causes a third-body abrasive effect at the contact interface.

To determine the tribological behavior of the samples, the adhesively worn surfaces are examined by SEM and EDS analysis (Fig. 7). The dominant wear mechanisms encountered in the samples are abrasive and oxidative. The EDS analyses of the C and CT samples show that spontaneously formed, Fe- and W-containing tribo-oxides are found in the worn surface (Fig. 7a point 4, Fig. 7b point1). These thick, compact tribo-oxides remain in direct contact with the hard counter body (WC ball) during dry sliding conditions. These oxide layers are very brittle and break in contact areas, due to the increasing wear distance. The oxide layers are separated from the surface and produce post-tribo-reaction products in the form of particles or strata, which remain between the contact surfaces during the test. These third bodies, which move on the interface, exacerbate the abrasive wear of the tribological system.

The CCT sample shows the lowest adhesive wear rate ( $1.38 \times 10^{-6} \text{ mm}^3/\text{Nm}$ ). The microstructure of this sample has been determined to have the highest secondary carbide precipitation and martensite phase ratio by XRD analysis (Figs. 1, 2). The wear resistance of this sample dramatically increases due to the effect of these secondary precipitated hard carbides. Also, the finer precipitated carbides formed provide a more homogeneous distribution. This homogeneous distribution increases the load-carrying capacity of the sample. On the worn surface of the CCT sample, cracks are seen less frequently compared to other worn samples (Fig. 7d). A small amount of W-containing thin oxide layers is observed in the SEM micrograph of the worn surface (Fig. 7d) compared to other samples. For this reason, the oxidative wear that occurs is partially reduced. The reduction in adhesive wear rate can be explained generally, by finer homogeneous precipitated wear resistive carbides resulting from the cryogenic treatment and tempering processes.

Figure 7 also exhibits the worn surface profile of the samples. The widest measured worn surface profile for each sample is given. It can be seen that the lowest worn

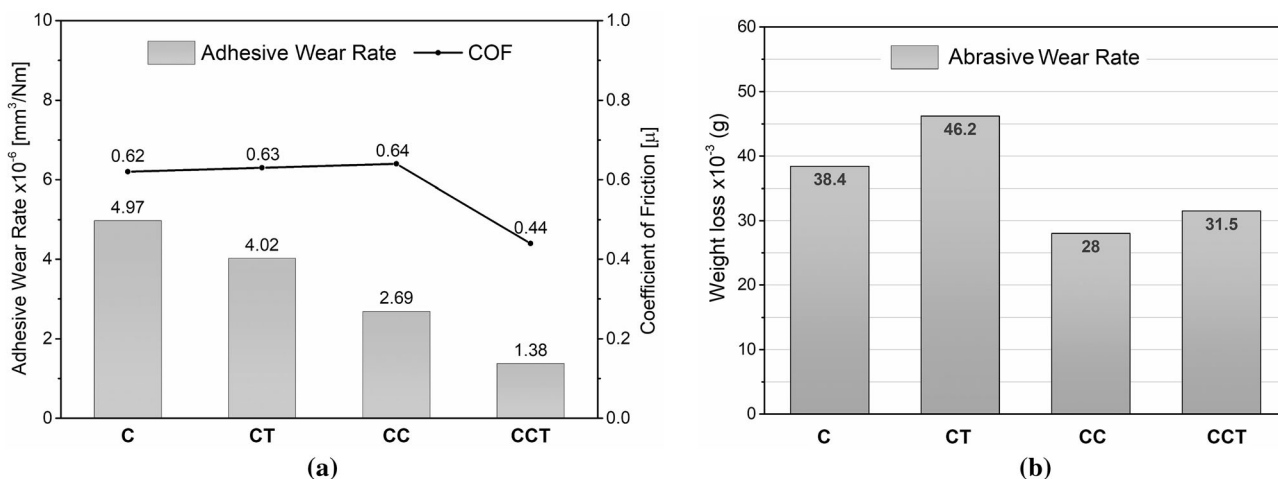


Fig. 5 Wear test results of the samples, a Adhesive wear rate and mean COF, b Abrasive wear rate

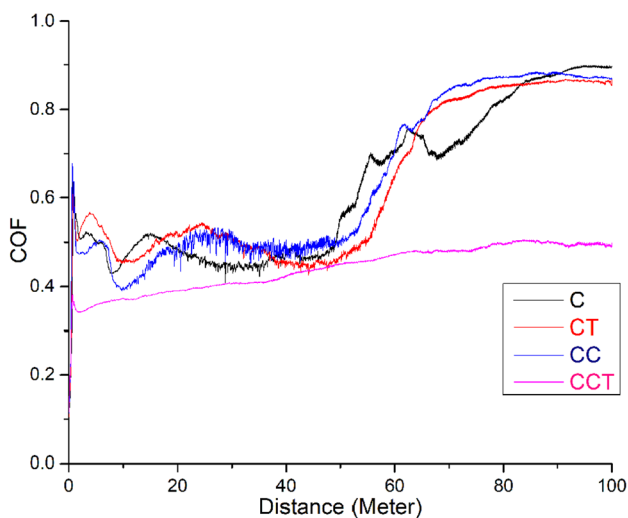


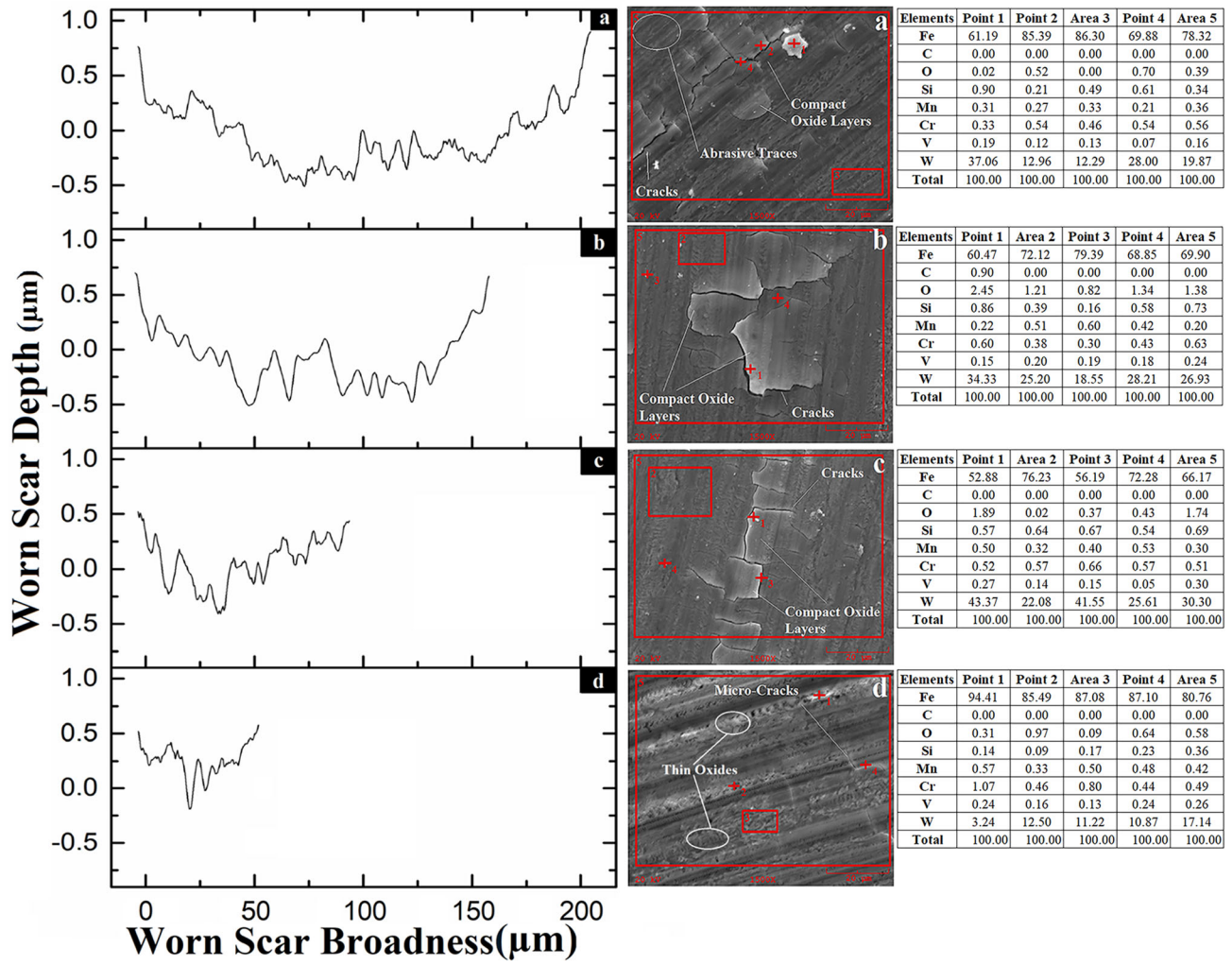
Fig. 6 COF versus adhesive wear distance of the samples

profile area is on CCT, while C shows the highest. Thin oxide layers are seen on the worn surface of CCT samples (Fig. 7d). These oxide layers remain without breaking, due to the homogeneous carbide distribution on the contact surfaces and the reduced wear rate.

Figure 8 shows a schematic illustration of the effect of carbides on the dry sliding adhesive wear test. The first case (Fig. 8a) examines the wear behavior of quenched conditions (C and CT), which have a dominantly rough primary carbide microstructure on a martensite matrix. In this case, the carbide grains are too coarse, and in such small amounts, that the coarse carbides cannot give enough support to the martensite matrix during wear. Therefore, surface deformations occur after coming in contact with the wear load (Fig. 8a). Furthermore, the friction coefficient and wear are exacerbated (Figs. 5a and 6) due to this situation. The second case (Fig. 8b) exhibits the contact

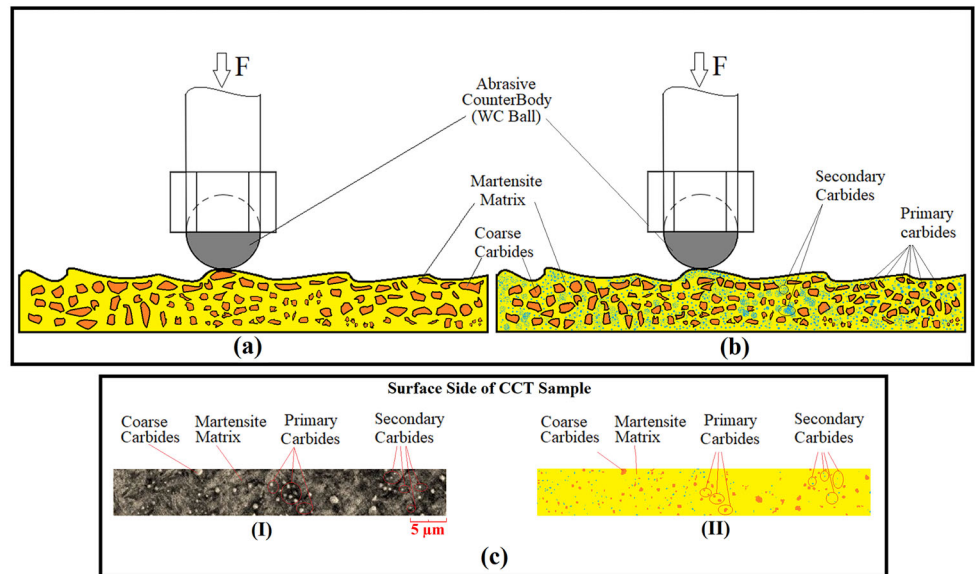
mechanism of the cryogenically treated conditions (CC and CCT) during the adhesive wear test. In this case, it can be seen that homogeneously secondary fine carbide is distributed throughout the microstructure, which increases the coinciding possibility of the abrasive counterpart (WC) at surface contact points. These precipitated carbide formations have a positive contribution to the adhesive wear resistance and coefficient of friction. The CCT sample provide the highest wear resistance due to the highest secondary carbide ratio and homogeneous carbide distribution in the microstructure. Figure 8c illustrates the surface SEM photograph and mapping analysis of the CCT sample. It is seen that the surface of the sample consists of mostly secondary carbides.

Abrasive wear test results, with regards to weight loss, are shown in Fig. 5b. This shows that cryogenic treatment reduces weight loss by approximately 1.37–1.65 times, as compared to conventional heat-treated conditions (C and CC). These results show that cryogenic treatment significantly improves the abrasive wear resistance. Figure 9 shows the highest measured worn surface profile and SEM micrographs of the abrasive worn surfaces of the samples. As expected, the highest and deepest worn scar is observed in the CT sample (Fig. 9b), while the CC sample shows the lowest performance (Fig. 9d). These results are in good correlation with the abrasive wear loss. It can be seen that there are wide abrasion marks, due to microplowing, on the worn surface of the C sample (Fig. 9a). From the EDS analyses, there is also oxide and wear debris present on the worn surface of this sample. It is clear that the as-quenched condition (C), does not exhibit sufficient resistance to abrasive wear due to the low-matrix rigidity. Therefore, the highest second weight loss among all the treated samples is observed in this sample.



**Fig. 7** The surface roughness of worn surface profile and SEM–EDS analyses of the adhesively worn samples **a** C, **b** CT, **c** CC, **d** CCT

**Fig. 8** Schematic illustration mechanism of the adhesive dry sliding wear test, **a** As-quenched conditions, **b** Cryo-treated Conditions, **c** Surface side of the CCT sample; **c-I** SEM photo of the CCT sample surface's, **c-II** Threshold SEM photo of the CCT sample surface's





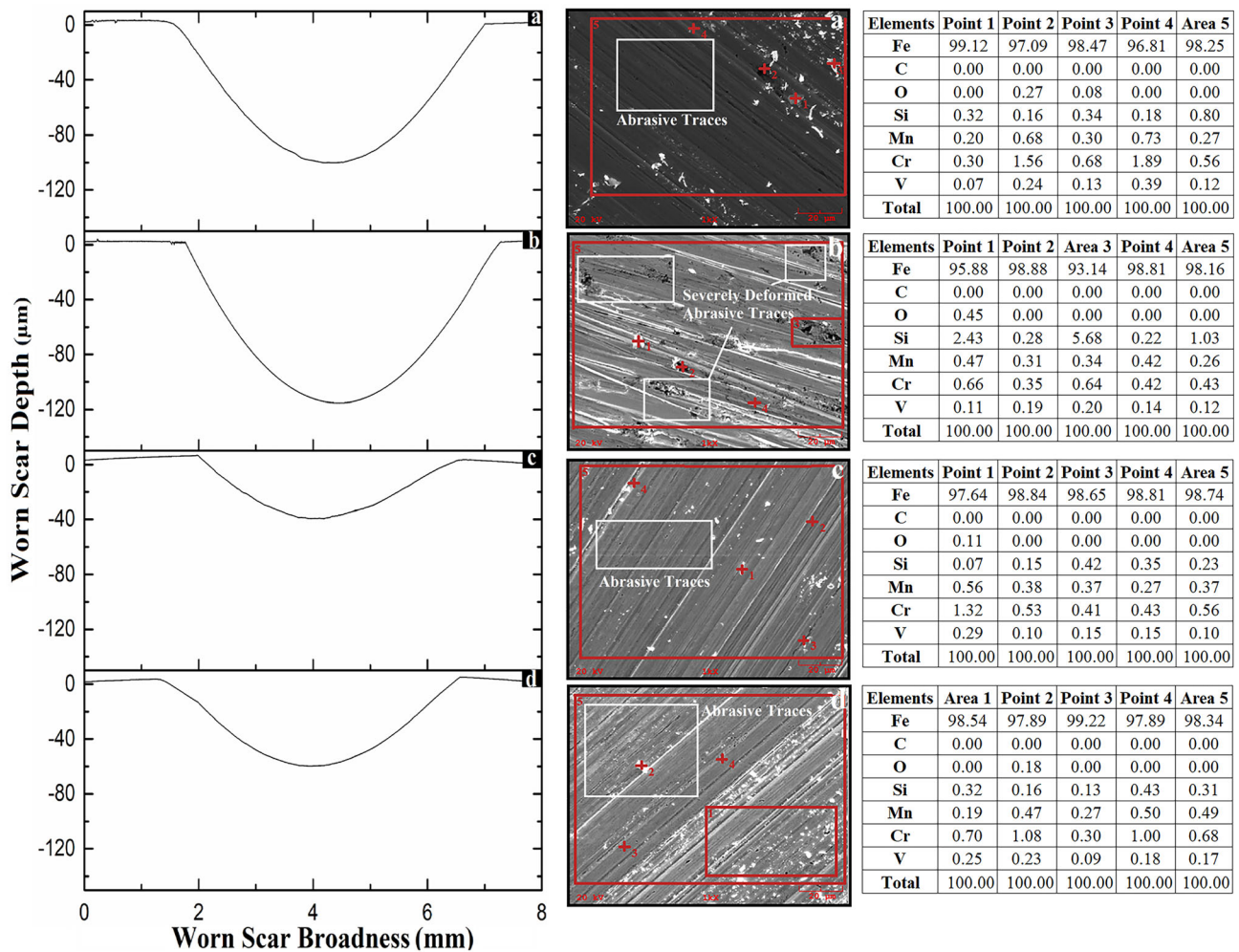


**Fig. 9** The surface roughness of worn surface profile and SEM-EDS analyses of the abrasively worn samples; **a** C, **b** CT, **c** CC, **d** CCT

The CT sample has the lowest hardness (62 HRC) due to the tempered martensite microstructure. SEM micrograph of the abrasive worn surface shows that there are wide wear-marks due to microplowings on the surface (Fig. 9b). It can also be seen that severely plastic deformed, Fe–Si containing, abrasive trace regions are in majority in the abrasive worn surface. These deformed structures on the surface increase real contact area and as such, exacerbate abrasive wear at the contact interface by increasing the particle breakage from the sample surface. Also, it is observed that the highest Si ratio, which is likely to come from the SiC sandpaper counter body, is found in this sample as 9.63% (Fig. 9b point 1 to 5). It shows that the tempering process, done after quenching, is not sufficient to contribute to the rigidity and abrasive wear resistance.

The lowest weight loss is observed in the CC sample as 28 mg. Very shallow abrasive traces are observed in the SEM micrograph of the sample’s worn surface (Fig. 9c) compared with those of the other groups. Due to the highest martensite matrix hardness of this sample (66 HRC), the

three-body abrasive particles, that are formed during the test can not penetrate the surface. This sample shows superior abrasive wear resistance to the other groups. It is expected that the weight loss of the CCT sample will be the lowest due to the high adhesive wear resistance. However, the CC sample shows better abrasive wear performance due to its high-hardness martensite matrix. As seen from the SEM micrograph of the abrasive worn surface (Fig. 9d), the hard particles formed during the experiment scratch the surface into microchannels. These scratches and the scratch related roughness, increase real contact areas at the interface, causing the deteriorating abrasive wear. However, the abrasive wear resistance of this sample is about 18–32% higher than the as-quenched conditions (C and CT). Although the CCT sample has high carbide density, abrasive resistance is lower compared to the CC sample due to low martensite matrix hardness. It is a known fact in the literature that the abrasive wear resistance of ferritic materials directly depends on the bulk hardness [21].

## 4 Conclusions

In this study, microstructural properties of AISI L2 cold work tool steel were improved by using a cryogenic treatment process. The microstructure, hardness, and tribological behaviors of the samples were investigated. The obtained results based on the experiments are summarized below:

- While C and CT samples contained lath martensite, austenite, coarse, and primary carbides, CC and CCT samples contained needle shaped martensite, a lesser ratio of austenite, primary, and secondary precipitated carbides.
- XRD tests showed that the retained austenite ratio was reduced seven times in the CCT sample. Besides, the peak intensities of martensite,  $M_7C_3$ ,  $M_2C$ , MC carbide phases were found to increase in the cryogenically treated samples (CC and CCT).
- Cryogenic treatment had enhanced the martensitic transformation. The main factor that increased the kinetics of carbide precipitation was found to be a tempering process applied after the cryogenic treatment. The highest density of carbides was found in CC and CCT samples, which resulted in their better tribological properties.
- The hardness values of the cryogenically treated samples were slightly increased ( $\approx$  4HRC) due to the martensitic transformation and secondary carbide precipitation.
- Cryogenic treatment reduced the distance between carbides and retained austenite ratio due to the formation of secondary carbides. However, this microstructural improvement affected the fracture toughness inversely.
- The lowest adhesive wear rate and COF were observed in the CCT sample. The adhesive wear rate was reduced 3.6 times by using the cryogenic treatment process.
- The CCT sample exhibited the lowest coefficient of friction behavior due to the coinciding possibility of the counterpart by the secondary fine carbides.
- The highest abrasive wear resistance was obtained in the CC sample (1.64 times). The CC sample was found to exhibit better abrasive wear resistance than the CCT sample due to the high-hardness martensite matrix. Also, it was found that the abrasive wear resistance of

the tool steels was directly related to the hardness of the main martensite matrix rather than the precipitated secondary carbides.

- It was also estimated that the CCT process would increase the operational service life of AISI L2 in mold-making applications due to high adhesive wear resistance, while the CC process provided the best solution for cold cutting operations due to the highest abrasive wear resistance.

## References

1. Li S, Xie Y and Wu X, *Cryogenics* **50** (2010) 89.
2. Korade D, Ramana K V and Jagtap K, *Trans Indian Inst Met* **22** (2019) e20170745
3. Gunes I, Cicek A, Aslantas K and Kara F, *Trans Indian Inst Met* **67** (2014) 909.
4. Li J, Min Y, Wang P, Cai X and Wu X, *Met Mater Int* **25** (2018) 546
5. Singh P J, Mannan S L, Jayakumar T and Achar D R G, *Eng Fail Anal* **12** (2005) 263.
6. Sivalingam V, Sun J, Selvam B, Murugasen P K, Yang B and Waqar S, *J Braz Soc Mech Sci* **41** (2019) 110
7. Shah N, Arora K, Dhokey N B, Dileep Kumar N and Tharian K T, *Tribol T* **62** (2019) 712
8. Liu H-H, Wang J, Shen B-L, Yang H-S, Gao S-J, Huang S-J, *Mater Des* **28** (2007) 1059.
9. Li B, Zhang S, Zhang T and Zhang J, *J Braz Soc Mech Sci* **41** (2018) 27
10. Araghchi M, Mansouri H and Vafaei R, *Mater Sci Tech Ser* **34** (2017) 468.
11. Ramesh S, Bhuvaneshwari B, Palani G S, Mohan Lal D, Mondal K and Gupta R K, *Vacuum* **159** (2019) 468.
12. Liu X, Zhao C and Zhao K, *Vacuum* **160** (2019) 394.
13. Senthilkumar D, *Adv Mat Res* (2018) 114
14. Shinde T and Dhokey N B, *Surf Eng* **33** (2017) 944.
15. Edelson B I and Baldwin J W M, *The Effect of Second Phases on the Mechanical Properties of Alloys*, Defense Technical Information Center, Belvoir (1959)
16. Leskovšek V, Ule B and Liščić B, *J Mater Process Tech* **127** (2002) 298.
17. Çiçek A, Kara F, Kivak T, Ekici E and Uygur İ, *J Mater Eng Perform* **24** (2015) 4431.
18. Li S, Min N, Deng L, Wu X, Min Y A and Wang H, *Mat Sci Eng A Struct* **528** (2011) 1247.
19. Das D, Ray K K and Dutta A K, *Wear* **267** (2009) 1361.
20. Li S, Min N, Li J, Wu X, Li C and Tang L, *Mat Sci Eng A Struct* **575** (2013) 51.
21. Moore M A, *Wear* **28** (1974) 59.

**Publisher's Note** Springer Nature remains neutral with regard to jurisdictional claims in published maps and institutional affiliations.